**7A.6** EXTREME WIND EVENTS OBSERVED IN THE 2002 THUNDERSTORM OUTFLOW EXPERIMENT

Kirsten D. Gast* and John L. Schroeder
Texas Tech University, Lubbock, Texas

## 1. INTRODUCTION

The flow characteristics of thunderstorm winds are not well understood. A number of studies have been conducted to analyze outflows and downbursts, namely the Joint Airport Weather Studies (JAWS), the Northern Illinois Meteorological Research on Downbursts (NIMROD) experiment (Fujita 1985), and single and dual Doppler observations (e.g. Parsons and Kropfli 1990, Klingle et al. 1987, Mueller and Carbone 1987, Wakimoto 1982). Valuable information about the general structure and behavior of outflows and downbursts has been obtained from these studies. Wakimoto (1982), for example, distinguished an outflow's life cycle, and Fujita (1985) classified downbursts based on their extent and pattern of surface divergence.

However, understanding of the fine-scale structure of the flow is lacking. This lack of understanding is in part due to the non-stationary nature of the flow, which limits the validity of analysis, particularly when applying traditional statistical analysis techniques. It is also due in part to the lack of high-resolution data, especially of extreme wind events.

The 2002 Thunderstorm Outflow Experiment was conducted from 20 May to 15 July to obtain high-resolution data of the kinematic and thermodynamic surface structure of thunderstorm outflows. Several outflows were recorded during the experiment, and two were of substantial intensity. The first event was produced by the rear-flank downdraft (RFD) of a nontornadic supercell on 5 June. The second event was a derecho generated by a mesoscale convective system (MCS) that caused wind-related damage from OK to the TX Gulf Coast on 16 June. The thermodynamic and kinematic analysis of these events will be discussed.

## 2. METHODOLOGY

### 2.1. *Experimental Setup*

Seven mobile, instrumented towers were deployed in a linear array from north to south equally spaced over a distance of 1578 m at the Reese Technology Center near Lubbock, Texas (Gast 2003). Four towers were 10 m, two were 3 m, and one was 15 m in height. The 15-m tower and one of the 10-m towers had instrumentation at multiple levels, while the rest of the towers measured data from one level.

*Corresponding author address: Kirsten D. Gast, Texas Tech Univ., Atmospheric Science Group, Lubbock, TX 79409; email: k.gast@ttu.edu.

All towers sampled at 2 Hz, except one 3-m tower, which sampled at 1 Hz (due to limitations of the data acquisition system).

A WSR-88D Doppler radar located 22 km away at the Lubbock International Airport supplied information about the parent thunderstorm. A West Texas Mesonet station was located only 30 m from the array. The calibrated data from this station was used to perform quality control and assurance on the experimental data.

### 2.2. *Analysis Procedures*

Each event exhibited specific structural features that were used to segment the data for analysis. The datasets were 1800-s time histories. The segments varied in length from 60 s to 600 s and were taken from a relatively stationary portion of the time history if possible.

Turbulence statistics, including gust factors (GF) and turbulence intensities (TI) were calculated for each segment. GF were calculated by taking the max 1-s gust and comparing it to the mean of the segment:

$$GF = \frac{\hat{U}_{1s}}{\overline{U}_T} \tag{1}$$

where $U$ represents the total wind (not longitudinal or lateral), and $T$ is the mean averaging time. TI were determined by comparing the standard deviation of the segment to its mean:

$$TI = \frac{\sigma_U}{\overline{U}_T} \tag{2}$$

Equivalent potential temperatures (theta-e) were calculated utilizing the Advanced Weather Interactive Processing System (AWIPS) method (UCAR):

$$\theta_e = \left( T + \frac{qL}{c_p} \right) \left( \frac{p_0}{p} \right)^{\frac{R}{c_p}} \tag{3}$$

where $T$ is the temperature (K), $q$ is the specific humidity, $c_p$ is the specific heat of dry air at constant pressure (J/deg Kg), $p_0$ is the standard reference pressure (mb), $p$ is the pressure (mb), $R$ is the gas constant (J/deg Kg), and $L$ is the latent heat of vaporization (J/Kg).

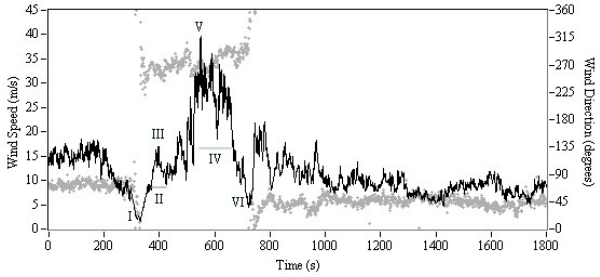


Figure 1. Wind speed (black) and direction (grey) time history of RFD. Start of event (I), IS (II), IG (III), PS (IV), PG (V), and downburst 'eye' (VI) are labeled.

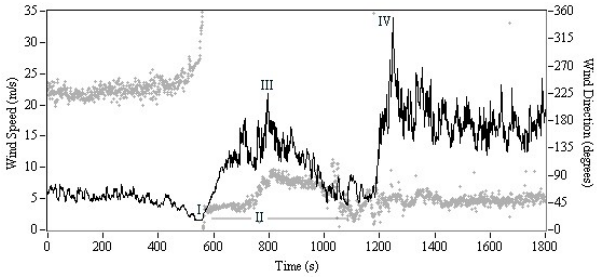


Figure 2. Wind speed (black) and direction (grey) time history of derecho. Start of event (I), IS (II), IG (III), and PG (IV) are labeled.

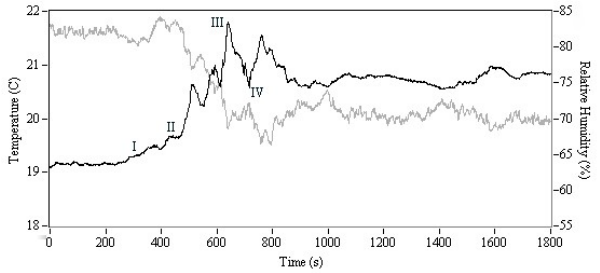


Figure 3. Fast-response temperature (black) and RH (grey) time histories of RFD. Start of event (I), IG (II), PG (III), and downburst 'eye' (IV) are labeled.

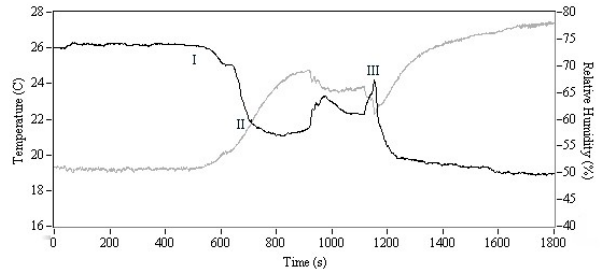


Figure 4. Fast-response temperature (black) and RH (grey) time histories of derecho. Start of event (I), IG (II), and PG (III) are labeled.

## 3. OBSERVATIONS

The RFD and derecho events were structurally similar in that they both exhibited an initial surge (IS), initial gust (IG), peak surge (PS), and peak gust (PG) as shown in Figures 1 and 2. However, the derecho lasted much longer than the RFD, mixing out and stabilizing

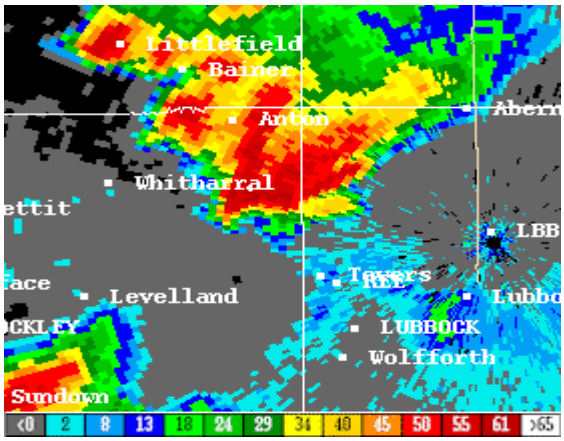


Figure 5. Base reflectivity from 1.4° elevation angle of supercell that generated RFD case at 0055 UTC 5 June.

over several hours. The RFD on the other hand lasted only about 6 min (360 s). The two events were thermodynamically different as well, as shown in Figures 3 and 4.

### 3.1 *Rear-Flank Downdraft*

Reflectivity data of the RFD event revealed that the parent supercell initiated at the intersection of a preexisting outflow boundary and a dryline. It initiated as an LP supercell, but quickly transitioned into a classic supercell as it propagated to the northeast. A fine-line echo was observed (Figure 5) as the gust front of the RFD progressed to the east.

The wind speed and direction time histories shown in Figure 1 revealed a sudden change in wind direction as the gust front passed through the tower array. The downdraft passed over the array as well, exhibited by the sudden change in wind direction after the peak surge. At the point of surface divergence the wind speeds of the downdraft diminish, only to increase again rapidly as the downdraft passes. Fujita (1983) observed this when he analyzed the Andrews AFB microburst, and referred to it as the 'eye' of the downburst. The wind speeds on the backside of the microburst were much greater in comparison to the RFD, likely due to the different angle of descent. The overall peak wind speed recorded for this event was 40 $ms^{-1}$ at 10 m.

### 3.2 *Derecho*

The parent thunderstorm developed in NW KS as a discrete supercell. It quickly transitioned into a mesoscale convective system (MCS) as it propagated to the SE. The leading edge bulged out to form a bow echo that surged to the S. The far western periphery of this system affected counties near Lubbock, TX (Figure 7). The MCS produced a number of outflows that merged into one large swath of damaging winds, but it was only the western fringe of the outflow that affected Lubbock County. The gust front of the outflow was evident on radar as shown in Figure 7.

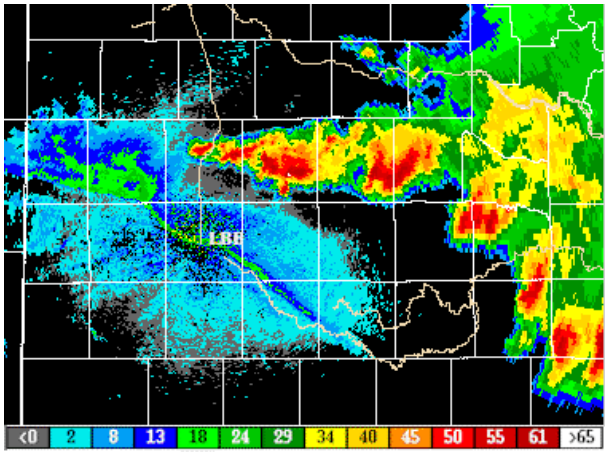

Figure 7. Base reflectivity from 0.5° elevation angle of MCS and derecho at 0410 UTC 16 June.

The wind direction for this case only shifted once as the gust front approached (Figure 2). The storm itself did not pass over the tower array so there was no secondary shift as was observed in the RFD case. The maximum wind speed recorded was 35 $ms^{-1}$ at 10 m.

### 3.3 *Statistical Comparison*

Given the non-stationarity of the data and the duration of the structural features, the greater the averaging time the more invalid the results become. In addition, the statistics become unstable when averaging times less than 120 s are utilized (Schroeder and Smith 2003). Figure 8 shows how the GF was affected by *T*. Choi and Hidayat (2002) noticed a similar linear relationship between *T* and GF values. Figure 9 is an example time history of GF values using a 1 s/ 120 s ratio. Choi and Hidayat also indicated that since TI was a function of the GF, TI values would increase as the GF increased. This indeed was true for these two cases as well (Figures 10-11). The peaks of the GF correspond directly with those of the TI. These peaks also correspond with data segments that are relatively non-stationary (where rapid increases in wind speed occur). See Table 1 for the statistical results.

### 3.4 *Thermodynamic Comparison*

The two events were thermodynamically different. The RFD produced a maximum temperature increase of 2.65 °C and relative humidity (RH) decrease of 20%. The mean temperature increase among the towers was 2.37 °C and mean RH decrease was 17%. Figure 3 shows a time history of temperature and RH from one of the towers during the RFD event. Figure 4 shows how the temperature and RH changed during the derecho event. The temperature decreased an average of 7.53 °C, while the RH increased an average of 29%. The maximum temperature decrease recorded was 8.30 °C, and the maximum RH increase was 33%.

Equivalent potential temperatures (theta-e) were calculated from the data obtained using the slow-response temperature (note that the fast-response

Table 1. Summary of turbulence statistics.

| *T* (s) | GF | | | TI | | |
|---|---|---|---|---|---|---|
| RFD | Mean | Max | Min | Mean | Max | Min |
| 60 | 1.35 | 1.99 | 1.13 | 0.17 | 0.56 | 0.06 |
| 120 | 1.47 | 2.04 | 1.18 | 0.21 | 0.54 | 0.08 |
| 180 | 1.56 | 1.94 | 1.22 | 0.25 | 0.45 | 0.10 |
| 240 | 1.59 | 2.15 | 1.32 | 0.26 | 0.47 | 0.13 |
| 300 | 1.67 | 1.99 | 1.43 | 0.29 | 0.45 | 0.17 |
| 360 | 1.64 | 1.98 | 1.42 | 0.29 | 0.42 | 0.19 |
| 420 | 1.66 | 2.02 | 1.42 | 0.28 | 0.41 | 0.17 |
| 480 | 1.90 | 2.20 | 1.59 | 0.34 | 0.45 | 0.21 |
| 540 | 2.19 | 2.69 | 1.40 | 0.37 | 0.49 | 0.19 |
| 600 | 2.07 | 2.44 | 1.49 | 0.34 | 0.50 | 0.21 |
| Derecho | | | | | | |
| 60 | 1.44 | 3.28 | 1.16 | 0.18 | 0.71 | 0.08 |
| 120 | 1.60 | 3.47 | 1.17 | 0.21 | 0.49 | 0.09 |
| 180 | 1.67 | 2.87 | 1.27 | 0.30 | 0.79 | 0.11 |
| 240 | 1.92 | 3.32 | 1.32 | 0.30 | 0.86 | 0.11 |
| 300 | 1.77 | 2.83 | 1.33 | 0.26 | 0.46 | 0.12 |
| 360 | 2.01 | 3.43 | 1.32 | 0.40 | 0.86 | 0.12 |
| 420 | 2.13 | 3.23 | 1.47 | 0.42 | 0.72 | 0.15 |
| 480 | 1.98 | 2.47 | 1.54 | 0.45 | 0.61 | 0.19 |
| 540 | 1.86 | 2.02 | 1.65 | 0.40 | 0.49 | 0.29 |
| 600 | 1.82 | 1.94 | 1.74 | 0.33 | 0.44 | 0.18 |

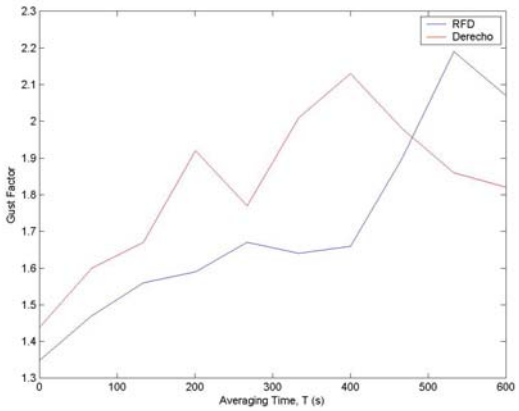

Figure 8. GF compared to averaging time.

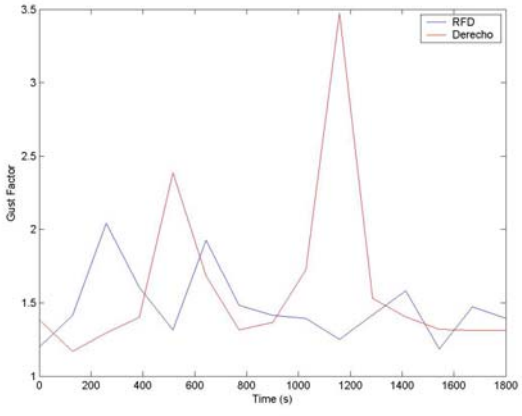

Figure 9. GF time histories for RFD and derecho. GF=1s gust/120s mean.

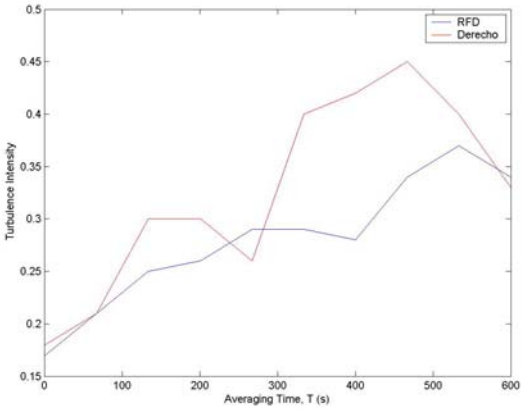


Figure 10. TI compared to averaging time.

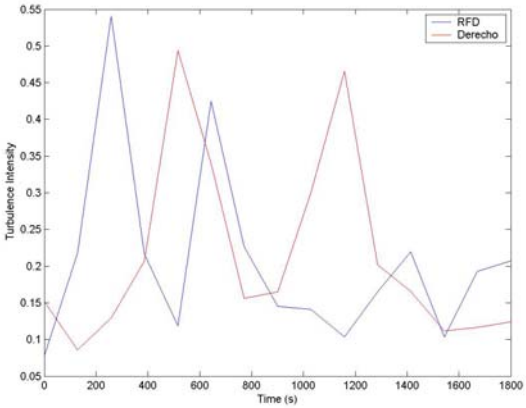


Figure 11. TI time histories for RFD and derecho. TI=st. dev./120 s mean.

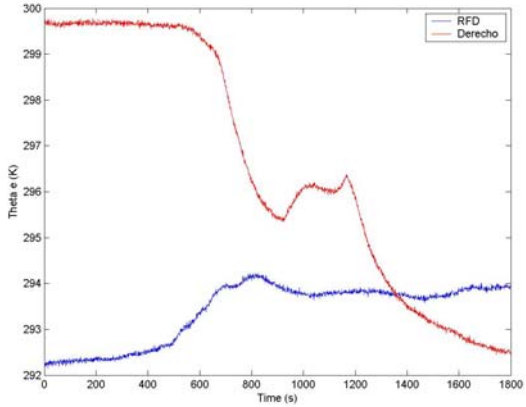


Figure 12. Theta-e 1-Hz time histories.

temperature data is shown in Figures 3 and 4). Figure 12 shows the theta-e time histories for each event. There was a decrease of theta-e observed for the derecho event, while there was an increase for the RFD event. Markowski (2002) observed a theta-e increase within the RFD of several tornadic supercells. This RFD case was associated with a nontornadic supercell.

## 4 *Conclusions*

The RFD and derecho exhibited similar kinematic structural features and an increase in gust factors and turbulence intensities. It seems apparent that the spikes in the statistics are a product of the non-stationarity of the data, but might also signify the actual nature of the flow. Such an increase in turbulence intensity could indicate that the turbulence was not predominately mechanically driven (a resultant of friction), particularly in the RFD event. Increased turbulence would be expected in the derecho case given the distance the outflow had propagated along the surface, but the RFD air had significantly less interaction with the surface and still generated turbulence intensity values similar to the derecho. Convective effects along the gust front may have also played a role in causing the high statistics.

There was an increase in temperature and theta-e during the RFD, and a decrease in temperature and theta-e due to the derecho. It is suspected that the height of origin and forcing mechanisms associated with the RFD event were different than those in the derecho case (Markowski et al. 2002).

## 5 *References*

Choi, C.C., F.A. Hidayat, 2002: Gust factors for thunderstorm and non-thunderstorm winds. *J. Wind Eng. Ind. Aerodyn.*, **90**, 1683-1696.

Fujita, T.T., 1983: Andrews AFB Microburst: Six Minutes After the Touchdown of Air Force One. SMRP Research Paper 205, University of Chicago, Chicago, Illinois, 38pp.

Fujita, T.T., 1985: The Downburst: Microburst and Macroburst. SMRP Research Paper 210, University of Chicago, Chicago, Illinois, 154pp.

Gast, K.D., 2003: A Comparison of Extreme Wind Events as Sampled in the 2002 Thunderstorm Outflow Experiment. Master's Thesis, Texas Tech Univ., Lubbock, Texas, 132pp.

Klingle, D.L., D.R. Smith, M.M. Wolfson, 1987: Gust front characteristics as detected by Doppler radar. *Mon. Wea. Rev.*, **115**, 905-918.

Markowski, P.M., J.M. Straka, E.N. Rasmussen, 2002: Direct surface thermodynamic observations with the rear-flank downdrafts of nontornadic and tornadic supercells. *Mon. Wea. Rev.*, **130**, 1692-1721.

Mueller, C.K., R.E. Carbone, 1987: Dynamics of a thunderstorm outflow. *J. Atmo. Sci.*, **44**, 1879-1898.

Parsons, D.B., R.A. Kropfli, 1990: Dynamics and fine structure of a microburst. *J. Atmo. Sci.*, **47**, 1674-1692.

Schroeder, J.L., D.A. Smith, 2003: Hurricane Bonnie wind flow characteristics as determined from WEMITE. *J. Wind Eng. Ind. Aerodyn.*, **91**, 767-789.

University Corporation for Atmospheric Research, 2004: Equivalent Potential Temperature, http://meted.ucar.edu/awips/validate/thetae.htm.

Wakimoto, R.M, 1982: The life cycle of thunderstorm gust fronts as viewed with Doppler radar and rawinsonde data. *Mon. Wea. Rev.*, **110**, 1060-1082.